



A robust state-of-charge estimator for multiple types of lithium-ion batteries using adaptive extended Kalman filter



Rui Xiong^{a,b}, Xianzhi Gong^b, Chunting Chris Mi^{b,*}, Fengchun Sun^a

^a National Engineering Laboratory for Electric Vehicles, School of Mechanical Engineering, Beijing Institute of Technology, No. 5 South Zhongguancun Street, Haidian District, Beijing 100081, China

^b Department of Electrical and Computer Engineering, University of Michigan, Dearborn, 4901 Evergreen Road, Dearborn, MI 48128, USA

HIGHLIGHTS

- Proposed a dynamic universal battery model based on second-order RC network.
- Proposed an AEKF-based SoC estimation approach with multiple closed loop feedback.
- Developed a SOC estimator for suitable for multiple lithium ion battery chemistries.
- Proved the system robustness and convergence behavior of SoC estimators.

ARTICLE INFO

Article history:

Received 12 March 2013

Received in revised form

12 June 2013

Accepted 13 June 2013

Available online 22 June 2013

Keywords:

Lithium-ion battery

Data driven

Dynamic universal battery model

Adaptive extended Kalman filter

State of charge

ABSTRACT

This paper presents a novel data-driven based approach for the estimation of the state of charge (SoC) of multiple types of lithium ion battery (LiB) cells with adaptive extended Kalman filter (AEKF). A modified second-order RC network based battery model is employed for the state estimation. Based on the battery model and experimental data, the SoC variation per mV voltage for different types of battery chemistry is analyzed and the parameters are identified. The AEKF algorithm is then employed to achieve accurate data-driven based SoC estimation, and the multi-parameter, closed loop feedback system is used to achieve robustness. The accuracy and convergence of the proposed approach is analyzed for different types of LiB cells, including convergence behavior of the model with a large initial SoC error. The results show that the proposed approach has good accuracy for different types of LiB cells, especially for C/LFP LiB cell that has a flat open circuit voltage (OCV) curve. The experimental results show good agreement with the estimation results with maximum error being less than 3%.

© 2013 Elsevier B.V. All rights reserved.

1. Introduction

Lithium ion battery (LiB) is currently considered the viable energy storage solution for electric and hybrid vehicles (HEV) for their high cell voltage, long cycle-life, high specific energy and high specific power [1]. For electric vehicles (EVs) and plug in hybrid electric vehicles (PHEVs), the state of charge (SoC) of the battery is a critical parameter as it reflects the remaining capacity in the battery pack, and is often used to implement the optimum control of charging and discharging processes. Thus, in order to manage the battery more efficiently, an accurate SoC estimation method is of paramount importance.

Several factors can impact the accuracy of SoC results, such as hysteresis phenomena between charge and discharge, characteristics of the open-circuit-voltage (OCV) over SoC, measurement noise, and limited current and voltage measurement accuracy [2]. Poor SoC estimation can result in unwanted overcharge or over discharge of the battery and lead to reduced battery calendar life and lower efficiency due to the complex and dynamic vehicle operation conditions [3]. There are many methods to estimate the SoC in electric and chemistry laboratories. Most of these methods depend on measurements of some convenient parameters which vary with SoC. Many of these methods need careful charge and discharge of the battery according to some predesigned pattern. The most challenging job in battery SoC estimation is then how to estimate SoC in the EVs without interruption of the vehicle operation [4]. The commonly used methods can be generally classified into four categories, namely, direct discharge method, coulomb counting method, voltage/impedance based method, and model based filter methods.

* Corresponding author. Tel.: +1 313 583 6434; fax: +1 313 583 6336.

E-mail addresses: rxiong6@gmail.com (R. Xiong), xianzhigong@gmail.com (X. Gong), chrismi@umich.edu, mi@ieee.org (C.C. Mi), sunfch@bit.edu.cn (F. Sun).

The first method is the **direct measurement method (discharge test)** [4–6]. This method depends on discharging the battery to obtain the amount of charge in the battery. There are three issues with this method. First, in most applications, the user (or the system) needs to know how much charge is in the cell without discharging it. Secondly, it is impossible to measure directly the effective charge in a battery by monitoring the actual charge put into the battery during charging due to the Coulomb efficiency of the battery.¹ Charge efficiency also depends on temperature and SoC. Thirdly, the measuring time is relatively long and this method can be only used in the laboratory and is not practical to implement the on-line estimation of batteries in vehicles.

The second method is the **current based SoC estimation – (Coulomb Counting) method** [7,8]. The energy contained in a battery is measured in Coulombs and the remaining capacity in a battery can be calculated by measuring the current flow rate (charging/discharging) and integrating (accumulating) over time. This method is often used as a core technology for battery SoC estimation in battery management systems (BMS). However, its performance is highly dependent on the measurement accuracy. This open-loop calculation method could be affected by accumulated calculation errors due to uncertain disturbances from the practical application and lack of necessary corrective resolution. Loss of initial SoC can cause the method to fail since the integration does not have a starting point.

The third one is the **voltage or impedance based SoC estimation method** which uses the voltage or impedance of the battery as the basis for calculating SoC or the remaining capacity [6,9–14]. Results can vary widely depending on actual voltage level, temperature, discharge rate and aging level of the cell. On one hand, problems can occur with some cell chemistries, especially for C/LFP LiB cell with flat OCV behavior. Ref. [4] shows that the maximum SoC variation per mV voltage for C/LFP battery is more than 5%. With the cell voltage measurement accuracy available today, the SoC error can be more than 20%. The rapid drop in cell voltage at the end of the cycle could be used as an indication of imminent. But for many applications, an earlier warning is required and fully discharging LiB cells will dramatically shorten their cycle life. Therefore, it is suitable only when electric vehicles are in idle mode rather than in drive mode. On the other hand, impedance based SoC estimations are not widely used due to difficulties in measuring the impedance while the cell is active as well as difficulties in interpreting the data since the impedance is also temperature dependent.

The last method is the **model-based method with filter algorithms or integrated algorithm based on multiple filters** [15–25]. Many SoC estimation methods based on the “black box” model have been proposed, such as artificial neural networks based models [15–17], fuzzy logic based models [18,19] and support vector regression (SVR) based models [20]. The robustness of these models strongly relies on the quantity and quality of the training data set. A limited training data set may result in limited model robustness, thus reducing the applicability of the model. On the other hand, more emphases have been placed on the methods which carry out estimation by means of state-space battery models. The number of papers about SoC estimation approach using Kalman filters and other observer-based approaches is increasing [5,11,21–25]. In Refs. [21–23], Gregory

L. Plett uses the extended Kalman filter (EKF) to adaptively estimate SoC based on a simplified battery model. However, the Kalman filter-based algorithm strongly depends on the precision of the battery model and the predetermined variables of the system noise such as mean value, relevance and covariance matrix. An inappropriate information matrix of the system noise may lead to remarkable errors and divergence [11]. Therefore, an adaptive extended Kalman filter (AEKF)-based method has been applied to implement online SoC estimation in Refs. [24,25] to improve the accuracy by adaptively updating the process and measurement noise covariance.

Although accurate SOC estimation is critical for vehicle power management and control [26–28], most of the estimation methods described above are validated using only one type of battery data, without applying to different types of batteries, different OCV behaviors and highly transient loading profiles. In other words, the robustness of these SoC estimation algorithms was not sufficiently assessed. For example, many SoC estimation approaches mentioned above were evaluated under one type of battery, such as lithium-ion polymer battery (LiPB) battery [21–23] whose OCV behavior is relatively steep so it is relatively easy to achieve precise state estimation accuracy and convergence behavior. But for LiFePO₄ battery, the convergence speed is much slower. Moreover, the performance and robustness of these SoC algorithms against different batteries were not adequately studied.

A key contribution of this paper is that a data driven-based robust SoC estimator for different types of LiB cells is proposed through the adaptive extended Kalman filter. The performance of the estimator against four types of LiB cells is sufficiently evaluated under highly transient loading profiles.

A description of the dynamic universal battery model, its parameter identification process and the data sets for the paper are given in Section 2. A data driven and AKKF algorithm based general SoC estimation approach is depicted in Section 3. The experiment and evaluation for the proposed estimation approach is illustrated in Section 4. Finally, the conclusion is presented in Section 5.

2. Battery modeling

2.1. The second-order RC network based dynamic universal battery model

For a model-based control system, the precision and complexity of the model are very important. The authors in Ref. [9] collected seven commonly used equivalent circuit models for batteries, including the *Shepherd* model, *Unnewehr Universal* Model, *Nernst* model, *combined* model, the *Rint* model, the first-order RC *Thevenin* model and the second-order RC model. The research showed that the second-order RC model has the highest precision and is more suitable for the voltage estimation of LiB cells. The authors in Ref. [29] use online parameter identification method to determine the relationship between the model accuracy and the number of RC networks, and concluded that the model with a second-order RC network has the best performance.

Based on the above results, the second-order RC model is selected in this paper. However, its open circuit voltage component of the circuit is replaced by an OCV function which takes SoC as the variable to strengthen the link between the model's performance and the battery SoC. The structure for the second-order RC network based dynamic universal battery model (abbreviated as *SRUB* model) is shown in Fig. 1. The electrical behavior of the proposed model can be expressed by Eq. (1). From Refs. [23], the simplified electrochemical function model is used to build the OCV functions as shown in Eq. (2).

¹ The Coulomb efficiency is the ratio of the number of charges that enter the battery during charging compared to the number of charges that can be extracted from the battery during discharging. The losses that reduce Coulomb efficiency are primarily due to the loss in charge due to secondary reaction. At low charge and discharge rate, the Coulomb efficiency is close to unity.

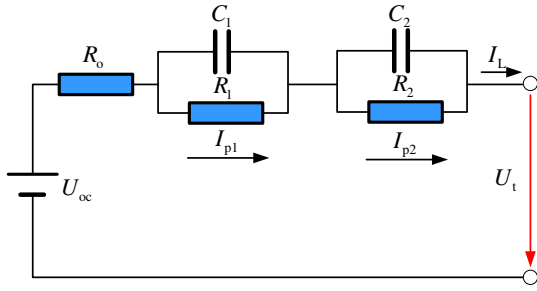


Fig. 1. Schematic diagram of the second-order RC based universal battery model.

$$\begin{cases} \dot{U}_1 = -\frac{1}{C_1 R_1} U_1 + \frac{1}{C_1} I_L \\ \dot{U}_2 = -\frac{1}{C_2 R_2} U_2 + \frac{1}{C_2} I_L \\ U_t = U_{oc} - U_1 - U_2 - I_L R_o \end{cases} \quad (1)$$

where U_{oc} is the open circuit voltage, and I_L is the load current (assumed positive for discharge, negative for charge), U_t is the terminal voltage, and R_o is Ohmic resistance. The second-order RC network is used to describe the relaxation effect (concentration polarization and electrochemical polarization performance) including the polarization resistance R_1 and R_2 , the polarization capacitance C_1 and C_2 . U_1 and U_2 are the polarization voltage across C_1 and C_2 respectively, I_{p1} and I_{p2} are the current flowing through the polarization resistance R_1 and R_2 respectively.

$$U_{oc} = K_0 + K_1 z + K_2/z + K_3 \ln z + K_4 \ln(1 - z) \quad (2)$$

where z stands for the SoC, K_i ($i = 0, 1, 2, 3, 4$) are the constants chosen to make the U_{oc} model fit the SoC–OCV data well.

2.2. Battery experiments

2.2.1. Battery test schedule

The test bench consists of an Arbin BT2000 Cycler with MITS Pro soft for programming the test process, a well-controlled temperature cabin and a host computer. The BT2000 has eight independent channels which can charge or discharge eight battery cells independently according to the designed profile with a maximum voltage of 5 V and a maximum current of 100 A in three scales (1 A/10 A/100 A). The measurement errors of the current and voltage sensors are less than 0.1%.

Four types of LiB cells are selected for the tests. The first one is the LiMn_2O_4 LiB cell which uses carbon (C) as its negative electrode and lithium manganese oxide (LMO) as its positive electrode (abbreviated as C/LMO). The second one is the $\text{Li}_4\text{Ti}_5\text{O}_{12}$ LiB cell which uses lithium titanate ($\text{Li}_4\text{Ti}_5\text{O}_{12}$) as its negative electrode and $\text{Li}[\text{NiCoMn}]\text{O}_2$ as its positive electrode (abbreviated as LTO/NCM). The third one is the $\text{Li}[\text{NiCoMn}]\text{O}_2$ LiB cell (abbreviated as C/NCM) and the last one is lithium iron phosphate the LiFePO_4 LiB cell (abbreviated as C/LFP). Their key specifications are shown in Table 1 (where the maximum available capacity is achieved by the tests

Table 1
Main specifications of the four types of LiB cells.

Lithium-ion battery cell	C/LMO	LTO/NCM	C/NCM	C/LFP
Nominal capacity (Ah)	35	20	35	1.35
Maximum available capacity (Ah)	34.5	19.1	36	1.23
Nominal voltage (V)	3.7	2.3	3.65	3.2
Upper cut-off voltage (V)	4.2	2.7	4.15	3.65
Lower cut-off voltage (V)	3.0	1.5	3.0	2.5

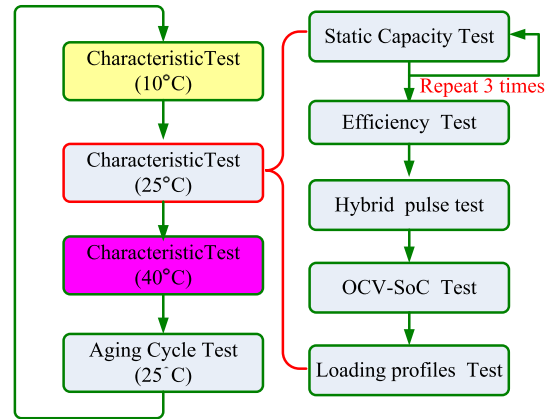


Fig. 2. Flowchart of the test schedule.

explained below). These cells were independently tested using the Arbin BT2000 battery cycler. The test schedules shown in Fig. 2 are designed to generate rich excitations for the four types of cells.

This paper focuses on the data sets collected at the temperature of 25 °C at one aging levels, and we plan carry out the research under different temperatures and aging levels in our future research.

2.2.2. Data sets

A static capacity test, a Coulombic efficiency test, a hybrid pulse test, an OCV vs. SoC test and loading profiles test are consecutively conducted in each characterization test. The purpose of the static capacity test is to measure the cell's maximum available capacity at its current state, which could be different from its nominal capacity due to the aging effect. The results are shown in Table 1.

The charge–discharge Coulomb efficiency test is used to get its Coulomb efficiency under different operation currents and then can be used to compensate the model and SoC estimation accuracy.

The specific hybrid pulse test is a sequence of pulse cycles. It is similar to the traditional hybrid pulse power characterization (HPPC) test, but the specific hybrid pulse test uses four different charge–discharge currents to improve the applicability of the SRUB battery model under a broader operation range of dynamic driving cycles. Because the HPPC only use 1C discharge and -0.75C charge currents, model error can be large due to the battery's current-dependent relaxation effect and Coulombic efficiency, etc. Considering that the operation ranges of the battery in EVs are typically less than 4C, we choose four currents (1C, 2C, 3C and 4C) to acquire identification data sets [5]. The sampling interval in the experiments is 1 s. The sampling current versus time of one cycle of specific hybrid pulse test is shown in Fig. 3.

The open circuit voltage measurement requires high precision (especially for C/LFP battery). Estimation of SoC and other battery states imposes more stringent requirements on cell voltage precision, especially on OCVs. In order to acquire data to identify K_i ($i = 0, 1, 2, 3, 4$) of the OCV function accurately, an OCV measurement test was performed on the above four types of LiB cells. The test procedure is as follows: (1) Fully charging the cells with CCCV (constant current constant voltage) charging mode, where the constant current is $C/3$ standard currents, the constant voltage is the cell's upper cut-off voltage and the cut off current is $C/20$. Then rest the cells for 5 h to finish the process of depolarization. (2) Discharging the cells with 5% of their maximum available capacity with a standard current. Afterward the cells were left in an open-circuit condition for 5 h to depolarize and then the measured terminal voltages were assumed to be their discharge OCV values. (3) Repeating the discharge method of step (2) until the cells reaches their lower cut-off voltage and after resting for 5 h their discharge

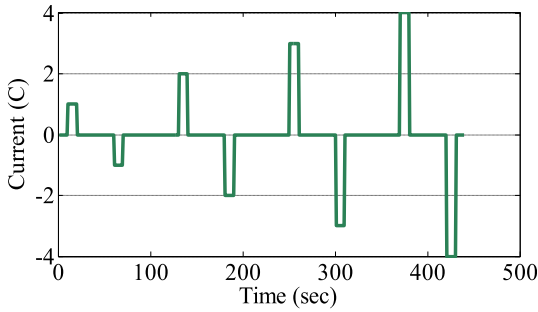


Fig. 3. The sampling current vs. time profile of one cycle of the specific hybrid pulse test.

OCVs are obtained. (4) Charging the cells for 5% of their maximum available capacity with CCCV charging mode, afterward the cells were rest in an open-circuit condition for 5 h to depolarize. Then the measured terminal voltages were assumed to be their charge OCV values. (5) Repeating the charging method of step (4) until their charging currents achieve C/20 amperes, and then their charged OCVs are obtained. (6) The average OCVs, the discharge OCVs and the charge OCVs have been obtained. Then the average OCVs are used to identify the parameters in Eq. (2), where the hysteresis is neglected to reduce model complexity.

Fig. 4 shows the OCVs of the four types of batteries as well as corresponding SoC variation per mV voltage. From Fig. 4(a) and (b), the slope of OCV curve of C/NCM is relatively steep and the maximal corresponding SoC rate of change per mV OCV is lower than 0.35% in the whole range. The slope of OCV curve of C/LMO and LTO/NCM are also relatively steep and the maximal corresponding SoC rate of change per mV OCV is lower than 0.4% in most range (except SoC 75–85% and 65–75%, respectively). Therefore, if the measurement precision of cell voltage is 10 mV, then the SoC error obtained through OCV estimation method could be lower than 4% in most SoC range. Accordingly, for C/LMO, LTO/NCM and C/NCM battery, the required measurement precision of cell voltage needs to be smaller than 10 mV. But the slope of OCV curve of C/LFP shown in Fig. 4(c) is relatively smooth. Hence, the maximal corresponding SoC rate of change per mV voltage reaches 1% in the commonly used SOC range as shown in Fig. 4(d). Therefore, the precision of cell

Table 2
Statistics of SoC variation per mV voltage (measured at 25 °C).

Lithium-ion battery cell	C/LMO	LTO/NCM	C/NCM	C/LFP
Maximum variation/mV ⁻¹	0.0042	0.0045	0.0033	0.0257
Mean variation/mV ⁻¹ (SoC = 0.3–0.8)	0.0024	0.0020	0.0019	0.0075
Maximum error with 5 mV	0.0210	0.0225	0.0165	0.1285
Mean error with 5 mV (SoC = 0.3–0.8)	0.0120	0.0100	0.0095	0.0375

voltage has more stringent requirement, reaching around 1 mV. At the present time, most test equipment collection precision of cell voltage can only reach 5 mV. Therefore the OCV-based SoC prediction is not sufficiently accurate. Table 2 shows the details of SoC variation per mV voltage and per 5 mV voltage.

From Table 2, the maximum SoC variation per mV voltage of C/LFP battery is 2.57%. Therefore, with 5 mV cell voltage measurement precision, the maximum SoC error can reach as high as 12.85%. As a result, the OCV-based SoC estimation for C/LFP is not efficacious. However, for the other three types of cells, the accuracy is acceptable when the cell voltage measurement precision is less than 5 mV with an accurate OCV vs. SoC map under different temperature and aging levels. Therefore, with a high tracking accuracy of battery terminal voltage, the OCV function should be able to model the OCV with acceptable precision.

In addition to the numerical study using synthetic data, the Federal Urban Driving Schedule (FUDS) cycle test is conducted to analyze the robustness and the reliability of the AEKF-based SoC estimation approach proposed in this paper. The FUDS profiles of the four types of battery are plotted in Fig. 5, in which the initial SoC of all batteries is set to 0.9 with discharge test under the standard current. In all cases, the “true” SoC is calculated from the Arbin test equipment data log using high precision Coulomb counting on measured data and compensating with the Coulomb efficiency. Note that the “true” SoC is only approximately accurate since current sensor error accumulated over time causes any estimation computed using coulomb counting to eventually diverge. It should be noted that, for different types of LIB cells, both the run time and the number of FUDS cycle are different because of their different operation currents. Specifically, when the maximum discharge current of a battery is more than 4C, the discharge time is relatively

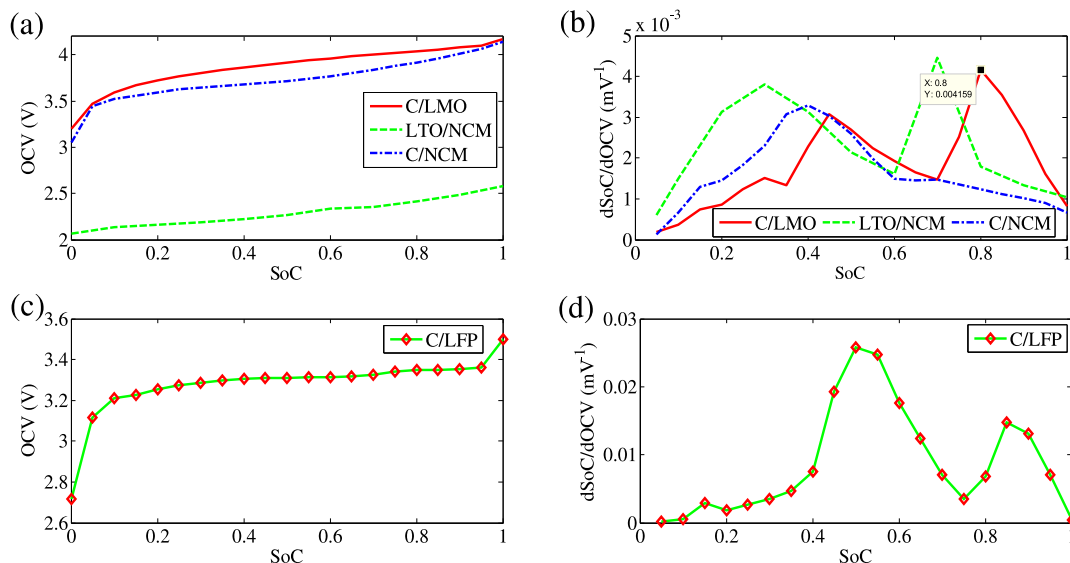


Fig. 4. OCV curves and SoC variation per mV OCV: (a) OCV maps of C/LMO, LTO/NCM and C/NCM lithium-ion batteries; (b) SoC variation per mV OCV of C/LMO, LTO/NCM and C/NCM lithium-ion batteries; (c) OCV map of C/LFP lithium-ion battery; (d) SoC variation per mV voltage of C/LFP lithium-ion battery.

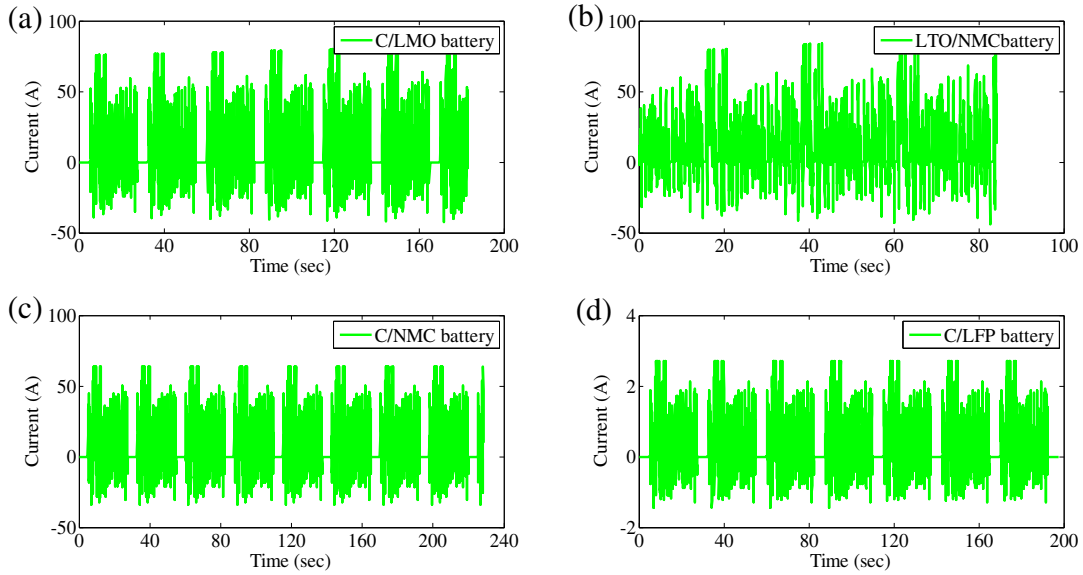


Fig. 5. Plots showing current vs. time for FUDS battery test, (a) current for C/LMO battery; (b) current for LTO/NCM battery; (c) current for C/NCM battery; (d) current for C/LFP battery.

short. Therefore, the continuous time of the LTO/NCM LiB cell is shorter than the other three types of LiB cells.

2.3. Parameter identification method

To identify the parameters of the *SRUB* battery model, we need to: (1) identify the parameters of OCV functions; (2) identify the ohmic resistance based on the pulse currents and pulse voltages; (3) discretize its electrical behavior equation shown in Eq. (1); (4) identify the dynamic voltage performance parameters of R_1 , R_2 , C_1 and C_2 .

Firstly, the parameters of the OCV functions are identified. Based on the SoC–OCV data shown in Fig. 4, the five constants for modeling OCV values under different SoCs and the correlation curves for the data and the model are shown in Table 3.

From Table 3, all the maximum errors of OCV model are more than 8 mV for C/LMO battery (assuming the measured OCV is accurate), LTO/NCM LiB cell and C/NCM LiB cell, especially for C/NCM LiB cell, whose error reached 30 mV. Furthermore, the maximum error occurs at the biggest SoC variation per mV voltage. For C/LFP LiB cell, the prediction precision of the OCV model is better than others due to its characteristic of OCV–SoC, but the SoC variation per mV voltage is much bigger than others.

Based on the above analysis, it can be concluded that the OCV based–SoC estimation with the SoC–OCV map is not very effective, even if the “true” OCV is achieved. The errors from the SoC–OCV

look-up table and the interpolation process will impact the SoC estimation results. In addition, the accuracy of the OCV-based SoC estimation method is highly dependent on the real-time estimation of its OCV. However, it is hard to provide a feedback or direct correction for the OCV with the measured values. The measurements only affect the prediction of the terminal voltage, which can hardly give an accurate adjustment for SoC estimation results. This method estimates the SoC in an open-loop way so the SoC estimation accuracy is limited. The SoC estimation performance can be worse when the battery has a flat OCV.

Secondly, identify the ohmic resistance based on the pulse currents and pulse voltages. The results are shown in Table 4 which listed the ohmic resistance values under the SoC ranges from 0.6 to 0.8. It can be seen from Table 4 that LTO/NCM LiB cell has the smallest ohmic resistance when converting the battery to the same capacity by parallel connection of the LiB cells. This is the reason that LTO/NCM battery has better power performance than others, and can be charged quickly.

Thirdly, the discretization form and regression equation for *SRUB* battery model is shown in Eq. (3).

where τ_1 ($\tau_1 = R_1 \times C_1$) and τ_2 ($\tau_2 = R_2 \times C_2$) are the time constants, which can be used to describe the relaxation effect of the power battery.

Lastly, identify the other model parameters, R_1 , R_2 , C_1 and C_2 . Provided that different τ_1 and τ_2 and different correlation coefficients can be calculated by using multiple linear regression method, the best

$$\begin{cases} U_{t,k} = U_{oc,k} - R_o I_{L,k} - R_1 I_{p1,k} - R_2 I_{p2,k} \\ I_{p1,k} = \left(1 - \frac{1 - \exp\left(\frac{-\Delta t}{\tau_1}\right)}{\left(\frac{\Delta t}{\tau_1}\right)} \right) I_{L,k} + \left(\frac{1 - \exp\left(\frac{-\Delta t}{\tau_1}\right)}{\left(\frac{\Delta t}{\tau_1}\right)} - \exp\left(\frac{-\Delta t}{\tau_1}\right) \right) I_{L,k-1} + \exp\left(\frac{-\Delta t}{\tau_1}\right) I_{p1,k-1} \\ I_{p2,k} = \left(1 - \frac{1 - \exp\left(\frac{-\Delta t}{\tau_2}\right)}{\left(\frac{\Delta t}{\tau_2}\right)} \right) I_{L,k} + \left(\frac{1 - \exp\left(\frac{-\Delta t}{\tau_2}\right)}{\left(\frac{\Delta t}{\tau_2}\right)} - \exp\left(\frac{-\Delta t}{\tau_2}\right) \right) I_{L,k-1} + \exp\left(\frac{-\Delta t}{\tau_2}\right) I_{p2,k-1} \end{cases} \quad (3)$$

Table 3
OCV function parameters and modeling accuracy.

Battery	OCV function parameters	OCV modeling accuracy
C/LMO	$\begin{cases} K_0 = 3.965 \\ K_1 = 0.123 \\ K_2 = 7.7 \times 10^{-5} \\ K_3 = 0.167 \\ K_4 = -0.009 \end{cases}$	
LTO/NCM	$\begin{cases} K_0 = 1.953 \\ K_1 = 0.554 \\ K_2 = -5.33 \times 10^{-6} \\ K_3 = -0.056 \\ K_4 = -0.007 \end{cases}$	
C/NCM	$\begin{cases} K_0 = 3.448 \\ K_1 = 0.565 \\ K_2 = -4.31 \times 10^{-6} \\ K_3 = -0.003 \\ K_4 = -0.012 \end{cases}$	
C/LFP	$\begin{cases} K_0 = 3.441 \\ K_1 = -0.132 \\ K_2 = 4.58 \times 10^{-6} \\ K_3 = 0.103 \\ K_4 = -0.017 \end{cases}$	

correlation coefficient is selected with accurate τ_1 and τ_2 . With the time constants, the model parameters R_1 , R_2 , C_1 and C_2 are estimated.

3. AEKF-based SoC estimation method

3.1. State of charge definition

SoC is a relative quantity that describes the ratio of the remaining capacity and the present maximum available capacity of a battery, given by:

$$z_k = z_0 - \frac{1}{C_n} \int_0^k \eta_i I_{L,t} dt \quad (4)$$

where z_k is the SoC at the k th sample time, z_0 is the initial SoC, $I_{L,t}$ is the instantaneous load current; η_i is the Coulomb efficiency, which

is a function of current and temperature. C_n is the maximum available capacity. The available SoC range is 0–100%. Since the sampling interval is 1 s, the unit of capacity calculated in Eq. (4) is A s.

The discretization of Eq. (4) is:

$$\text{SoC}_k = \text{SoC}_{k-1} - \frac{\eta_i I_{L,k} \Delta t}{C_n} \quad (5)$$

where Δt represents the sampling interval. Eq. (5) is the basis of the iterative calculation of SoC.

3.2. The adaptive extended Kalman filter algorithm

The extended Kalman filter has been widely used for parameter identification and state estimation in battery systems [21–25].

Table 4
Identification results of ohmic resistance (SoC = 0.6–0.8).

SoC/Battery	C/LMO (mΩ)	LTO/NCM (mΩ)	C/NCM (mΩ)	C/LFP (mΩ)
0.60	0.951	0.399	2.349	66.772
0.65	0.955	0.401	2.341	65.598
0.70	0.960	0.403	2.351	64.597
0.75	0.964	0.411	2.312	63.869
0.80	0.968	0.419	2.303	63.235

However, its performance is heavily reliant on the accuracy of the predetermined noise matrix. As a result, due to the complex and various operation environments of electric vehicles, the Kalman filter based battery control system has not been used in practice. To overcome this problem, an adaptive extended Kalman filter (AEKF) approach employing the covariance matching is applied to the state estimation in this paper [30].

In order to apply AEKF for the SoC estimation, it must first have a system model in a state-space form. Specifically, we assume a very general framework for discrete-time lumped dynamic systems.

$$\mathbf{x}_{k+1} = \mathbf{A}\mathbf{x}_k + \mathbf{B}\mathbf{u}_k + \omega_k \quad (6)$$

$$\mathbf{y}_{k+1} = \mathbf{C}\mathbf{x}_{k+1} + \mathbf{D}\mathbf{u}_k + v_k \quad (7)$$

where \mathbf{x}_k is the system state vector at the k th sampling time. It represents the total effect of system inputs \mathbf{u}_k on the present system operation, such as SoC. ω_k is the unmeasured “process noise” that affects the system state and v_k is the measurement noise which

does not affect the system state, but can be reflected in the system output estimation \mathbf{y}_k . ω_k is assumed to be Gaussian white noise with zero mean and covariance \mathbf{Q}_k ; v_k is assumed to be Gaussian white noise with zero mean and covariance \mathbf{R}_k . The matrices \mathbf{A} , \mathbf{B} , \mathbf{C} and \mathbf{D} describe the dynamics of the system, and are time varying and determined by looking up the parameters table.

An implementation flowchart of the AEKF algorithm is shown in Fig. 6. The AEKF provides a further innovation using the filter’s innovation sequence and the innovation allows the parameters \mathbf{Q} and \mathbf{R} to be estimated and updated iteratively.

3.3. SoC estimation with AEKF algorithm

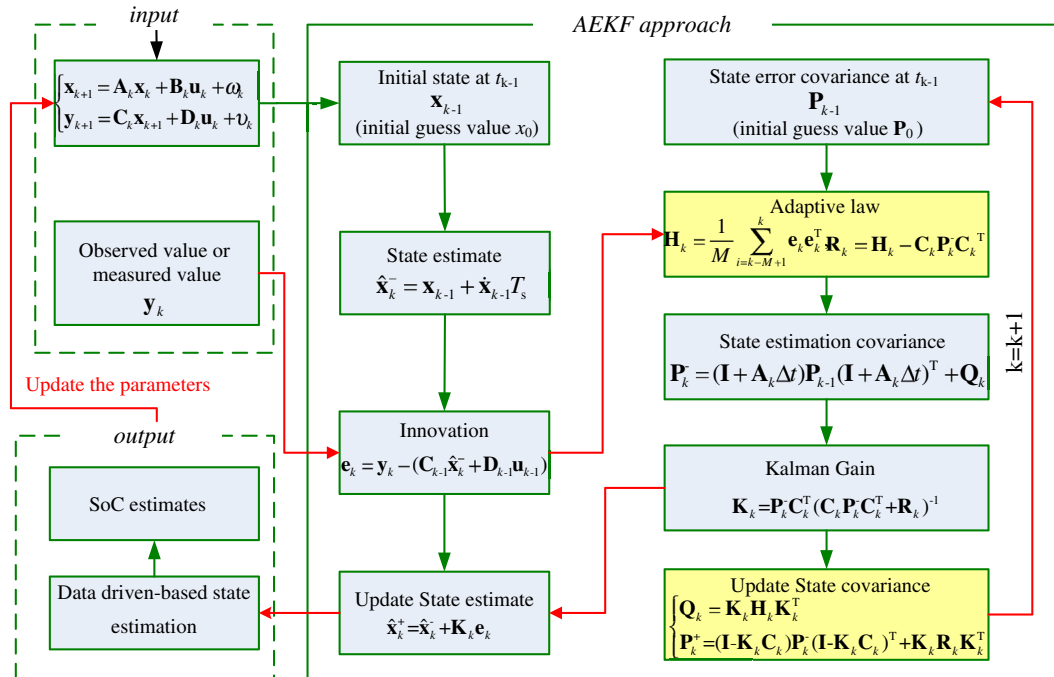
Transform Eq. (1) to a discrete system:

$$\begin{cases} U_{1,k} = U_{1,k-1} \exp(-\Delta t/\tau_1) + I_{L,k-1}R_1(1 - \exp(-\Delta t/\tau_1)) \\ U_{2,k} = U_{2,k-1} \exp(-\Delta t/\tau_2) + I_{L,k-1}R_2(1 - \exp(-\Delta t/\tau_2)) \\ U_{t,k} = U_{oc} - I_{L,k}R_o - U_{1,k} - U_{2,k} \end{cases} \quad (8)$$

Then the state \mathbf{x} , observation matrix \mathbf{y} and input matrix \mathbf{u} are defined as follows:

$$\begin{cases} \mathbf{x}_k = [U_{1,k} \ U_{2,k} \ z_k]^T \\ \mathbf{y}_k = U_{t,k} \\ \mathbf{u}_k = I_{L,k} \end{cases} \quad (9)$$

The time varying matrices \mathbf{A} , \mathbf{B} , \mathbf{C} and \mathbf{D} are defined as follows:



Note: \mathbf{H}_k is the innovation covariance matrix based on the innovation sequence inside a moving estimation window of size M . \mathbf{Q}_k and \mathbf{R}_k for the \mathbf{Q} and \mathbf{R} at the k th sampling time respectively. Where \mathbf{K}_k is the kalman gain matrix; \mathbf{e}_k is defined as the difference between the measurement and the observation $\mathbf{C}_{k-1}\hat{\mathbf{x}}_k^- + \mathbf{D}_{k-1}\mathbf{u}_{k-1}$; $\hat{\mathbf{x}}_k^-$ and $\hat{\mathbf{x}}_k^+$ are for the *priori* estimate *before* the measurement is taken into account and the *posteriori* estimate after the measurement is taken into account respectively. t_{k-1} is the initial time of calculation.

Fig. 6. The implementation flowchart of the AEKF algorithm.

$$\mathbf{A}_k = \begin{pmatrix} \exp\left(\frac{-\Delta t}{\tau_1}\right) & 0 & 0 \\ 0 & \exp\left(\frac{-\Delta t}{\tau_2}\right) & 0 \\ 0 & 0 & 1 \end{pmatrix}, \mathbf{B}_k = \begin{pmatrix} R_1 \left(1 - \exp\left(\frac{-\Delta t}{\tau_1}\right)\right) \\ R_2 \left(1 - \exp\left(\frac{-\Delta t}{\tau_2}\right)\right) \\ \frac{\eta_1 \Delta t}{C_n} \end{pmatrix} \quad (10)$$

$$\mathbf{C}_k = \frac{\partial U_t}{\partial \mathbf{x}} \Big|_{\mathbf{x}=\hat{\mathbf{x}}_k} = [-1 \quad -1 \quad \frac{dU_{oc}(z)}{dz} \Big|_{z=\hat{z}_k}], \mathbf{D} = [-R_0] \quad (11)$$

where, $dU_{oc}(z)/dz = K_1 - K_2/z^2 + K_3/z - K_4/(1-z)$ from Eq. (2).

The data driven based SoC estimation method with AEKF algorithm is shown in Fig. 7. The FUDS cycle based charge–discharge currents are loaded into the LiB cells and the battery model simultaneously. Terminal voltage error between the observer and the experimental data is adaptively reduced by updating the Kalman gain matrix K_k . The noise matrixes and Kalman gain are updated with the innovation error e_k . Then the updated gain is used to compensate for the state estimation error. The SoC estimation is fed back to update the parameters of the battery model for the SoC estimation at the next sampling time.

4. Verification and discussion

This section presents the verification and evaluation of the SRUB model-based SoC estimation approach with AEKF algorithm for four types of LiB cells.

4.1. State of charge estimation

Firstly, the prediction precision of the AEKF-based terminal voltage of the four types of LiB cells is discussed. Provided that the initial state \mathbf{x}_0 and covariance matrix \mathbf{P}_0 is known, the terminal voltage can be calculated in real-time. The terminal voltage estimation values and their errors are plotted in Fig. 8.

From Fig. 8, the estimated terminal voltage tracks the experimental profiles well, and the details are shown in the zoomed figures. It indicates that the terminal voltage error is generally within 3% of their actual voltage. The reason is that the AEKF-based algorithm can precisely estimate the voltage and timely adjust the Kalman gain according to the terminal voltage error between the measured and estimated values. In additional, it can be found that the SRUB model applied for C/LFP LiB cell has the best model accuracy, while the worst performance is seen for LTO/NMC and C/NCM battery. This is mainly due to the battery OCV performance and material characteristics. C/LFP LiB cell has the inconspicuous varying characteristic in its OCVs under different SoCs, and as a result, for a big error of SoC, the OCV difference is not obvious. Therefore, the C/LFP LiB cell always have a better modeling accuracy than the other three types of LiB cells in terms of terminal voltage estimation. However, the C/LFP LiB cell has the most sensitive characteristic in terminal voltage errors as shown in Figs. 4 and 8. It can be found that the bigger terminal voltage errors of C/LFP battery can cause unacceptable SoC errors. As a result, the better modeling accuracy of the C/LFP LiB cell cannot suggest that the precision is better than others. In contrary, LTO/NMC LiB cell has a worse modeling accuracy but has a better control accuracy than C/LFP LiB cell. For LTO/NMC and C/NCM LiB

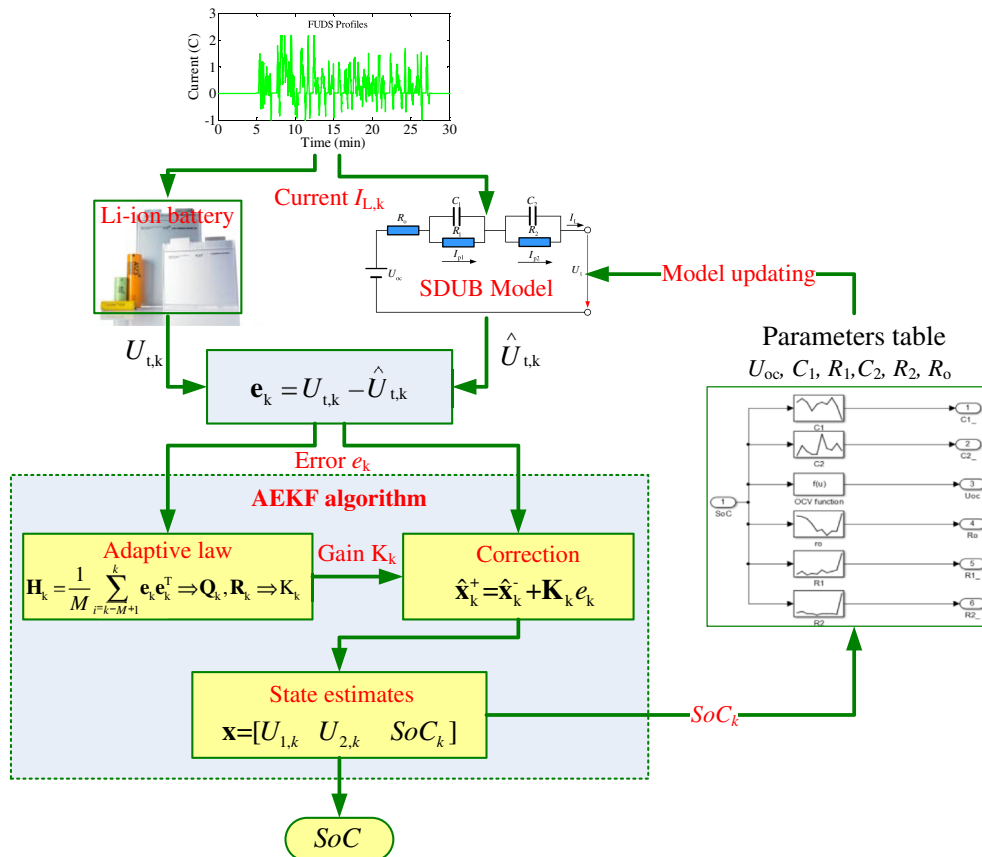


Fig. 7. The implementation flowchart of the data driven-based SoC estimation approach with AEKF algorithm.

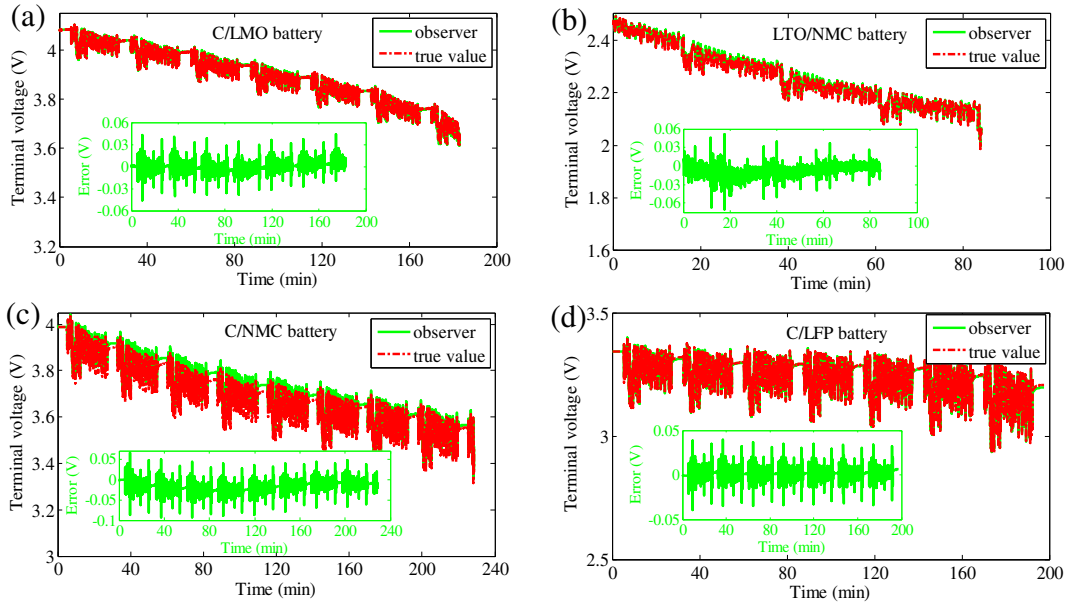


Fig. 8. AEKF-based terminal voltage estimation and its error. (a). C/LMO battery; (b). LTO/NCM battery; (c). C/NCM battery; (d). C/LFP battery.

cells, their performances are mainly dependent on their materials, including nickel, cobalt and manganese of their anode which have different performance. Hence, the OCV behavior is different from the LiB cell which has only one material for the anode. As a result, the OCV curves can be divided into three parts and therefore, the model accuracy is worse than others. However, from Fig. 4, the state estimation accuracy is not very sensitive to its voltage measurement error.

Secondly, we will discuss the SoC prediction precision for the four types of LiB cells with known initial SoC. The SoC estimation values and their errors are plotted in Fig. 9.

From Fig. 9, all the SoC estimation errors are less than 3% with a known initial SoCs. For different kinds of LiB cells, the SoC calculation precision is different. Therefore, the SoC estimation accuracy proved from a single type of LiB cell is not sufficient to represent the others.

However, an accurate SoC estimation depends on two factors according to the definition of SoC given by Eq. (5). One is the initial SoC, and the other is the calculation of SoC consumption. In order to investigate whether the proposed SoC estimation approach is effective with unknown or wrong initial SoC, a further simulation analysis on the AEKF approaches is conducted. Lastly, two different wrong initial SoC, 0.98 and 0.60, are pre-set and the corresponding SoC estimations are performed based on the FUDS cycles.

4.2. Robustness analysis

The SoC estimation results and their estimation errors with two wrong initial SoCs are shown in Fig. 10–13. Fig. 10(a) is the comparison among the SoC estimation with two erroneous initial SoCs and the reference SoC trajectory for C/LMO LiB cell. Fig. 10(b) is the

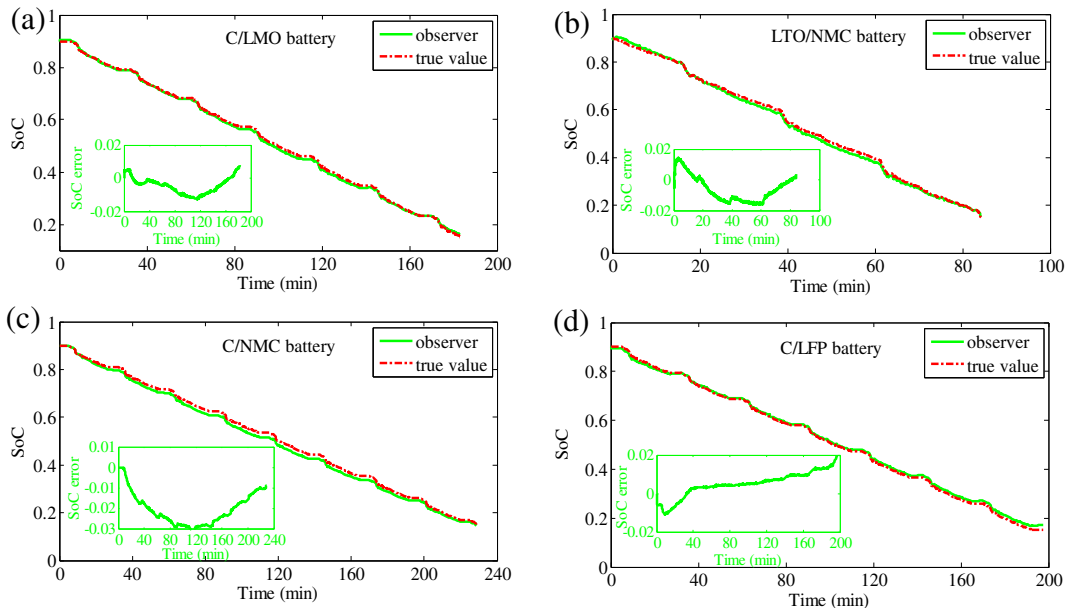


Fig. 9. AEKF-based SoC estimates and their error: (a). C/LMO battery; (b). LTO/NCM battery; (c). C/NCM battery; (d). C/LFP battery.

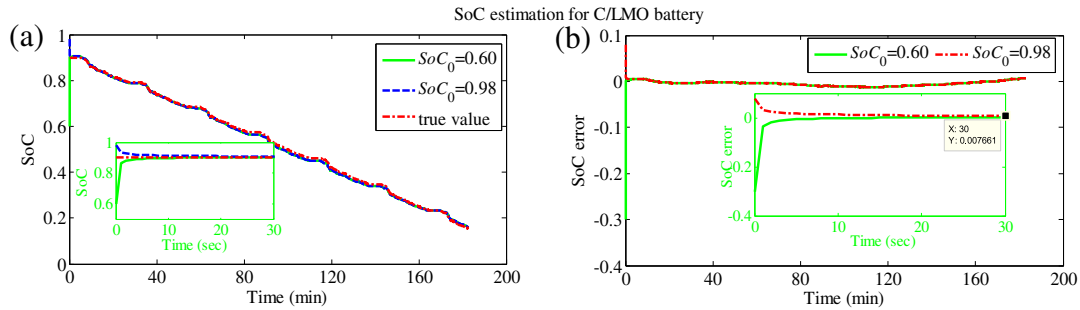


Fig. 10. Robust performance evaluation results for C/LMO battery. (a). SoC estimation results; (b). SoC estimation error.

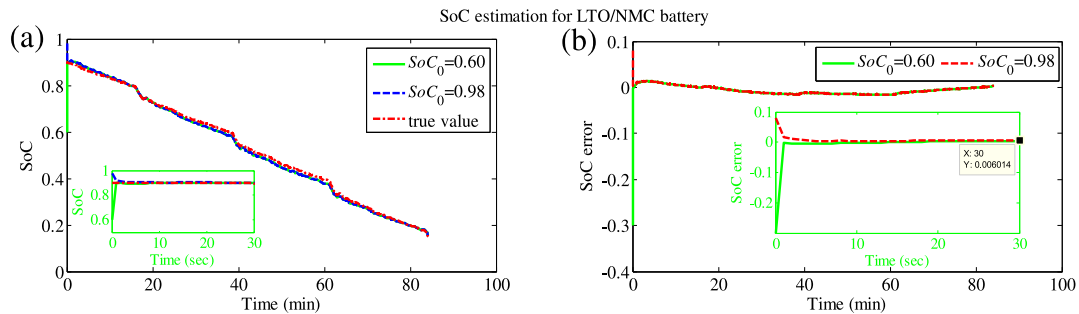


Fig. 11. Robust performance evaluation results for LTO/NMC battery. (a). SoC estimation results; (b). SoC estimation error.

SoC estimation error for the two erroneous initial SoCs. From Fig. 10(a), the SoC estimation can trace the true trajectory accurately and quickly especially with the large initial SoC error. Furthermore, from the zoomed figure of Fig. 10(a), the SoC estimation can converge to the reference SoC trajectory with several sampling intervals. From Fig. 10(b), for different large initial SoC errors, the SoC estimation can converge to the true value after several sampling intervals. That is because the proposed approach can precisely estimate the voltage and adjust timely the Kalman gain according to the error between the measured and estimated terminal voltage. The error SoC brings bigger terminal voltage errors, which will in turn cause a big Kalman gain matrix and then compensate the SoC estimation in an efficient closed loop feedback. Therefore it can obtain the accurate SoC estimation even with a large initial SoC error. Therefore, the proposed data driven-based SoC estimation approach can effectively trace the SoC trajectory even with a large initial SoC error, with the SoC estimation error in the whole SoC operation range being less than 2%.

Fig. 11(a) is the comparison between the SoC estimation with two wrong initial SoCs and the true SoC for LTO/NMC LiB cell. Fig. 11(b) is the SoC estimation error for the two erroneous initial SoCs. From

Fig. 11, the tracking accuracy of the proposed SoC estimation approach is very good for LTO/NMC cells, with the SoC estimation error in the whole SoC operation range being less than 2%. In addition, the convergence speed is faster than the C/LMO LiB cell.

Fig. 12(a) is the comparison between the SoC estimation with two erroneous initial SoCs and the true SoC for C/NMC LiB cell. Fig. 12(b) is the SoC estimation error for the two erroneous initial SoCs. From Fig. 12, the SoC estimation can trace the true SoC accurately, and the SoC estimation can converge to the true value after certain sampling intervals. Therefore, the proposed SoC estimation approach can effectively estimate the SoC for LTO/NMC LiB cell with the SoC estimation error in the whole SoC operation range being less than 3%.

Fig. 13(a) is the comparative profiles between the SoC estimation with two erroneous initial SoCs and the true SoC for C/LFP LiB cell, Fig. 13(b) is the SoC estimation error for the two initial SoCs. From Fig. 13, the SoC estimation results can trace the true SoC accurately, and the SoC estimation can converge to the true value after certain sampling intervals. Therefore, the proposed SoC estimation approach can effectively estimate the SoC for C/LFP LiB cell with SoC estimation error in the whole SoC operation ranges being less than

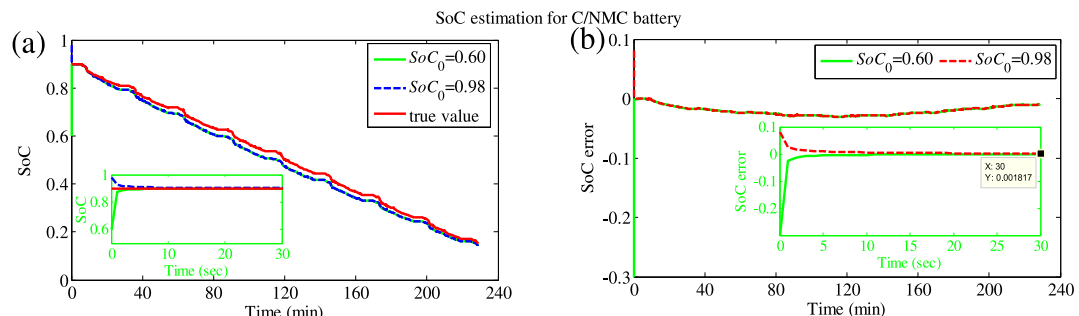


Fig. 12. Robust performance evaluation results for C/NMC battery. (a). SoC estimation results; (b). SoC estimation error.

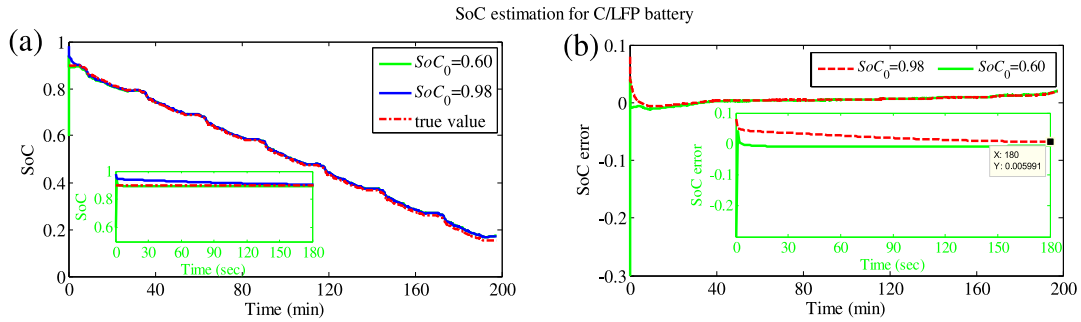


Fig. 13. Robust performance evaluation results for C/LFP battery. (a). SoC estimation results; (b). SoC estimation error.

Table 5
Statistic results of convergence performance of SoC estimation error after several sampling intervals.

Battery	C/LMO	LTO/NCM	C/NCM	C/LFP
Maximum error	0.0077 (0.0077)	0.0143 (0.0140)	0.0018 (0.0011)	0.0195 (0.0200)
Minimum error	-0.0126 (-0.0126)	-0.0163 (-0.0163)	-0.0299 (-0.0299)	-0.0062 (-0.0113)
Mean error	-0.0045 (-0.0046)	-0.0061 (-0.0062)	-0.0195 (-0.0193)	0.0055 (0.0050)
Variance	2.5e-05 (2.4e-05)	7.1e-05 (7.0e-05)	6.2e-05 (6.1e-05)	2.4e-05 (3.9e-05)

The values before the bracket are results for initial SoC of 0.98, and the values inside the bracket are results for initial SoC of 0.60.

2%. However, the convergence behavior is slower than the above three types of LiB cells for its OCV characteristic.

Table 5 lists SoC estimation error after several continuous sampling intervals. For C/LFP LiB cell, the interval is 180 s but for the other three types of LiB cells, the interval is 30 s. This is used to evaluate the performance of the proposed data driven-based SoC estimation approach for different types of LiB cells.

It can be found that the convergence performances of the proposed approach for the four types of LiB cells are satisfactory, even with large initial SoC errors. In addition, for different initial SoC errors, the convergence values and accuracies are almost the same. Therefore, the proposed data driven-based SoC estimation approach can still be effective even with inaccurate or wrong initial SoC and trace the reference or true SoC accurately. However, for different types of LiB cells, the prediction precisions and convergence behavior are different.

Based on the above analysis, it can be found that the prediction precision and convergence behavior of the proposed data driven-based SoC estimation with AEKF approach are accurate for different LiB cells. The maximum errors are less than 3%; and the C/LMO LiB cell has the best terminal voltage and SoC estimation precision. It is noted that with a more appropriate and accurate battery model applied to C/NCM LiB cell, the estimation accuracy will be improved. Therefore, the estimation accuracy of model-based terminal voltage and SoC depends on a few factors, including the type of battery, its material characteristic and open circuit voltage performance. In addition, the accurate battery model and estimation approach are both important.

5. Conclusions

Based on the above analysis, the main concluding remarks can be drawn:

- (1) To accurately model the dynamic performance of LiB cells, the second-order RC network based dynamic universal battery model is employed for SoC estimation. The electrochemical model is used to build the relationship between SoC and the open circuit voltage characteristics of the battery. The model has the advantages of high accuracy for the terminal voltage,

and can improve SoC estimation accuracy through an efficient closed-loop feedback.

- (2) To precisely predict the SoC, we have analyzed the relationship between SoC and OCV. The results show that the maximum SoC variation per 5 mV voltage of C/LFP LiB cell is 12.85%, and other types are approximately 2%. However, the present measurement precision of cell voltage is 10 mV in most BMS, and as a result, the SoC estimation based on the online OCVs or voltage measurement is not efficacious. Therefore, multi-parameter-closed loop feedback mechanism is necessary to build an efficient model-based BMS to improve the battery control accuracy.
- (3) To build an accurate and generic SoC estimation approach for different types of batteries, we have built an AEKF algorithm-based data-driven robust SoC estimation on the basis of the proposed dynamic universal battery model, which uses the OCV and five other model parameters to build the closed-loop feedback system and to correct the error from only using the OCV to estimate the SoC.
- (4) To analyze the robustness and the reliability of proposed data driven-based SoC estimation approach, we have conducted the Federal Urban Driving Schedule (FUDS) cycle test for different types of LiB cells. The results indicate that the proposed approach not only has the advantages of online estimating the terminal voltage accurately and reliably, but also can predict the SoC accurately with high robustness, with peak errors for terminal voltage and SoC all less than 3%.

Our future work will focus on the joint estimation approach with different structures of the battery pack, and the systematic validation test scheme for available peak power capability estimation.

Acknowledgments

This work is partially supported by the US DOE Grant DE-EE0002720 and DE-EE0005565, the Higher education innovation intelligence plan (“111” plan) of China and Graduate School of Beijing Institute of Technology in part.

References

- [1] C. Mi, A. Masrur, D.W. Gao, *Hybrid Electric Vehicles: Principles and Applications with Practical Perspectives*, Wiley, 2011.
- [2] J. Li, J. Barillas, C. Guenther, M. Danzer, *J. Power Sources* 230 (2013) 244–250.
- [3] X. Hu, S. Li, H. Peng, F. Sun, *J. Power Sources* 217 (2012) 209–219.
- [4] L. Lu, X. Han, J. Li, J. Hua, M. Ouyang, *J. Power Sources* 226 (2013) 272–288.
- [5] R. Xiong, H. He, F. Sun, X. Liu, Z. Liu, *J. Power Sources* 229 (2012) 159–169.
- [6] Pop, H. Bergveld, D. Danilov, Paul P.L. Regtien, Peter H.L. Notten, *Battery Management Systems: Accurate State-of-Charge Indication for Battery-Powered Applications*, Springer, Netherlands, 2008.
- [7] Y. Hu, S. Yurkovich, *J. Power Sources* 198 (2012) 338–350.
- [8] R. Xiong, H. He, F. Sun, K. Zhao, *Energies* 5 (2012) 1455–1469.
- [9] H. He, R. Xiong, H. Guo, S. Li, *Energy Convers. Manage.* 64 (2012) 113–121.
- [10] J. Kim, G. Seo, C. Chun, B. Cho, S. Lee, 2012 IEEE Int. Electric Veh. Conf. (IEVC) (March, 2012) 1–5.
- [11] R. Xiong, H. He, F. Sun, K. Zhao, *IEEE Trans. Veh. Technol.* 62 (2013) 108–117.
- [12] D. Deperneta, O. Bab, A. Berthon, *J. Power Sources* 219 (2012) 65–74.
- [13] Jamie Gomez, Ruben Nelson, Egwu E. Kalu, Mark H. Weatherspoon, Jim P. Zheng, *J. Power Sources* 196 (10) (2012) 4826–4831.
- [14] Alvin J. Salkind, Pritpal Singh, A. Cannonea, Terrill Atwater, Xiquan Wang, David Reisner, *J. Power Sources* 116 (2003) 174–184.
- [15] T. Weigert, Q. Tian, K. Lian, *J. Power Sources* 196 (2011) 4061–4066.
- [16] T. Wu, M. Wang, Q. Xiao, X. Wang, *Smart Grid and Renewable Energy* 3 (2012) 51–55.
- [17] Y.L. Murphey, J. Park, L. Kiliaris, M.L. Kuang, M.A. Masrur, A.M. Phillips, Q. Wang, *IEEE Trans. Veh. Technol.* 62 (2013) 69–79.
- [18] P. Singh, C. Fennie, D. Reisner, *J. Power Sources* 136 (2004) 322–333.
- [19] Souradip Malkhandi, *Eng. Appl. Artif. Intel.* 19 (2006) 479–485.
- [20] Q.-S. Shi, C.-H. Zhang, N.-X. Cui, *Int. J. Automot. Technol.* 9 (2008) 759–764.
- [21] G.L. Plett, *J. Power Sources* 134 (2004) 252–261.
- [22] G.L. Plett, *J. Power Sources* 134 (2004) 262–276.
- [23] G.L. Plett, *J. Power Sources* 134 (2004) 277–292.
- [24] J. Han, D. Kim, M. Sunwoo, *J. Power Sources* 188 (2009) 606–612.
- [25] J. Wang, J. Guo, L. Ding, *Energy Convers. Manage.* 50 (2009) 3182–3186.
- [26] M. Zhang, Y. Yan, C.C. Mi, *IEEE Trans.* 61 (2012) 1554–1566.
- [27] B. Zhang, C.C. Mi, M. Zhang, *IEEE Trans.* 60 (2011) 1516–1525.
- [28] X. Zhang, C. Mi, *Vehicle Power Management: Modeling, Control and Optimization*, Springer, London, 2011.
- [29] H. He, X. Zhang, R. Xiong, Y. Xu, H. Guo, *Energy* 39 (2012) 310–318.
- [30] G. YE, P.P. SMITH, J.A. NOBLE, *Ultrasound Med. Biol.* 36 (2010) 234–249.